# CHAPTER 20

# Characteristics of absorbing directional wavemaker

H. Hirakuchi [1] , R.kajima, T.Shimizu, M.Ikeno

## ABSTRACT

In order to maintain realistic and expected incident waves, an absorbing directional wavemaker has been developed and its performance is examined experimentally. The directional spectrum of the generated waves in the progressive wave field is analysed by the Bayesian Model (BDM), and the directional spectrum of the incident waves in the combined wave field is separated by the Modified Bayesian Model (MBM). Good agreement is shown between the BDM result and the MBM result. In order to make a further check on the angular spreadings of the directional waves in the progressive and combined wave fields, coherence function of the cross spectrum is measured and compared with the target one derived theoretically.

# 1    Introduction

Hydraulic model tests have often been conducted to solve the various problems associated with the planning and the design of coastal structures. It is very important to reproduce realistic ocean surface waves in a laboratory basin. Majour hydraulic laboratories in the world have built the directional wavemakers during the last decade.

To generate short-crested waves by the directional wavemaker, several different random wave synthesis methods have been developed. All of these synthesis methods are based on the simulation of the irregular waves which have the specific directional spectrum. For evaluating the performance of the directional wavemaker, the directional spectrum analysis becomes of importance. Several analysis models are proposed and used for this purpose.

---

[1]Abiko Research Laboratory, Central Research Institute of Electric Power Industry, 1646 Abiko, Abiko-shi, Chiba, JAPAN   277-11

However, it is well known that each model gives the different result, although the same data are used. Therefore, it is very important to use another analysis method except for the directional spectrum analysis method as well as to select the best directional analysis model.

When a model structure is highly reflective and occupies a large part of a width of a basin, re-reflected waves at a paddle affect the incident waves. In the case of the 2-D experiment, an absorbing wavemaker has been developed and used in a wave channel (Hirakuchi et al., 1990b). In order to maintain better controlled wave conditions in a incident and reflected combined wave field, an absorbing directional wavemaker has been developed. To evaluate the absorption performance of the developed wavemaker, it is important to separate the directional spectrum of the incident waves from the combined wave field. For this purpose, Isobe and Kondo(1986) modified the MLM technique, and Hashimoto et al.(1987a) proposed the Modified and the Extended Bayesian Model (MBM and EBM). The separated result would be also affected by the resolution power of each model.

The purpose of this study is to examine the performance of the absorbing directional wavemaker experimentally. We first consider some aspects of the usefulness of the coherence function of the cross spectrum, for evaluation of the wave angular spreadings. Next, we carry out the several experiments in the progressive wave field and the combined wave field with regular and irregular waves, and make comparison of the wave height and the directional spectrum. A further check on the wave spreadings of the generated waves are obtained by comparing the coherence distribution in space and frequency domain.

# 2     Coherence function of directional wave field

Directional wave field used in a wave modelling is usually represented by the following form:
$$S(f, \theta) = P(f) \cdot G(\theta; f) \tag{1}$$
where $S$, $P$ and $G$ are the directional spectrum, the frequency spectrum and the angular spreading function, respectively. In the case of Mitsuyasu-type spreading function, $G$ is:
$$G_M(\theta) = \frac{(2s)!!}{2\pi (2s - 1)!!} \left( \cos \frac{\theta - \theta_0}{2} \right)^{2s} \tag{2}$$
where $\theta_0$ is the mean wave angle, and $s$ is the angular spreading parameter. In this paper, $s$ is defined as:
$$s = \begin{cases} s_{max} (f/f_p)^5 & ; f \leq f_p \\ s_{max} (f/f_p)^{-2.5} & ; f \geq f_p \end{cases} \tag{3}$$

where $f_p$ is a peak frequency of the power spectrum and $s_{max}$ is a maximun value of the spreading parameter at $f_p$.

The general relationship between the directional spectrum and the cross spectrum can be expressed as:

$$\phi_{mn}(\sigma) = \int_{\boldsymbol{k}} H_m(\boldsymbol{k},\sigma) H_n^*(\boldsymbol{k},\sigma) S(\boldsymbol{k},\sigma) \exp(-i\boldsymbol{k} \cdot \boldsymbol{r}_{mn}) d\boldsymbol{k} \qquad (4)$$

where $\phi_{mn}$ is the cross-spectrum between the point $\boldsymbol{x}_m$ and $\boldsymbol{x}_n$, $\boldsymbol{r}_{mn}$ is a space vector ($\boldsymbol{r}_{mn} = \boldsymbol{x}_n - \boldsymbol{x}_m = (R\cos\alpha,\ R\sin\alpha)$ ), $H$ is the complex transfer function relating the water surface elevation to any wave quantity, and '*' represents the complex conjugate value.

When the wave quantities measured are wave surface elevations, $H$ is $H_m = H_n^* = 1.0$. In this case, the cross spectrum can be expressed as:

$$\phi_{mn}(\sigma)/P(\sigma) = C_1 - i\,Q_1 \qquad (5)$$

$$C_1 = J_0(kR) + 2 \sum_{j=1}^{[s/2]} \frac{s!\,s!\,(-1)^j\,J_{2j}(kR)}{(s-2j)!\,(s+2j)!}\ \cos(2j\delta) \qquad (6)$$

$$Q_1 = -2 \sum_{j=0}^{[(s-1)/2]} \frac{s!\,s!\,(-1)^j\,J_{2j+1}(kR)}{(s-2j-1)!\,(s+2j+1)!}\ \cos(2j+1)\delta \qquad (7)$$

where $C_1$ and $Q_1$ are co-spectrum and quadrature spectrum, respectively, $J$ is a Bessel function and $\delta$ is:

$$\delta = \alpha - \pi - \theta_0 \qquad (8)$$

The cross spectrum is often expressed by the coherence and the phase:

$$coh = \frac{|\phi_{mn}|^2}{\phi_{mm}\,\phi_{nn}} \qquad (9)$$

$$phs = \tan^{-1}\left(\frac{\text{Imag}\,(\phi_{mn})}{\text{Real}\,(\phi_{mn})}\right) \qquad (10)$$

Fig.1 is an example of the spacial distribution of the coherence function between the origin and any other position in the directional wave field with the spreading parameter of s=10 and 75. It is shown that the coherence value along the main wave direction from the origin keeps very heigh value, although the coherence value along the wave crest line from the origin decreases very rapidly. In the case of uni-directional waves, the coherence value should be 1.0 all over the field. Therefore, it can be said that the decreasing rate of the coherence value in space domain reflects the angular spreadings of the directional wave field.

In Fig.1, the coherence value along the crest line from the origin becomes less than 0.1 over the range of $R/L > 2$, where $L$ is a wave length. It means
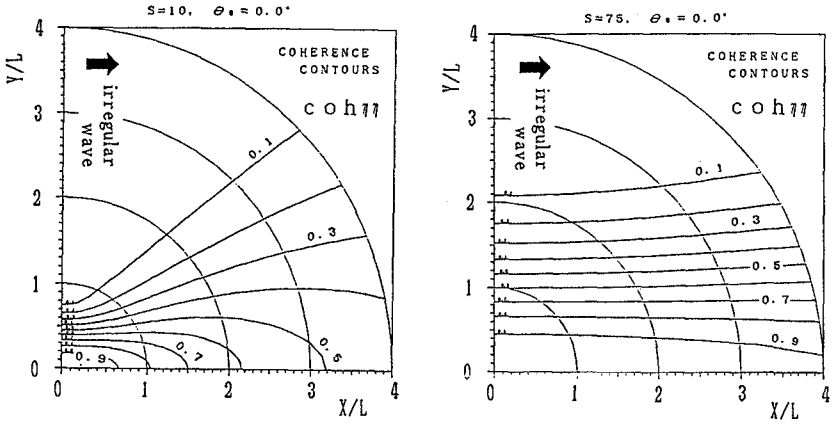
(a) $s = 10$                                      (b) $s = 75$

**Fig.1**   Coherence distribution in the progressive wave field.
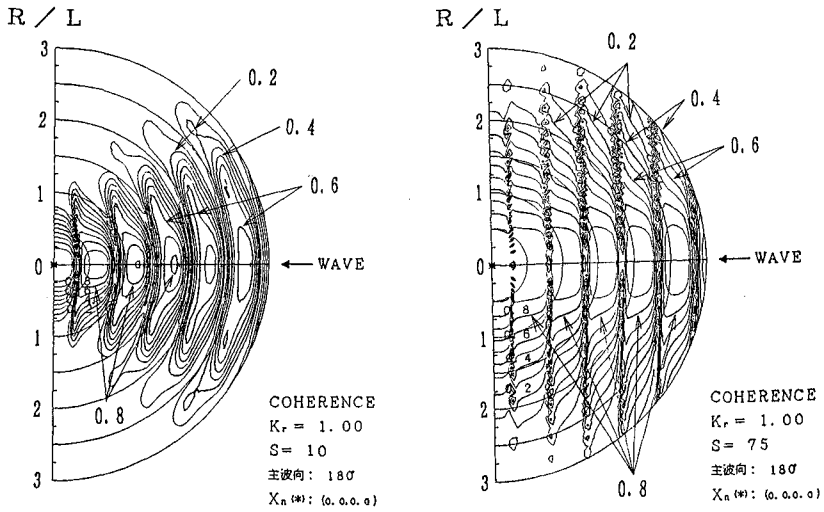


(a) $s = 10$                                      (b) $s = 75$

**Fig.2**   Coherence distribution in the combined wave field.

that the data measured at two points with the distance of $R/L > 2$ along the wave crest line are statistically independent. It also means that it is possible to get the ststistically independent cross spectra by arranging the several wave arrays, each of which is located with the distance of $R/L > 2$ along the wave crest line.

The relationship between the crosss and directional spectrum in the incident and reflected combined wave field is derived by Isobe and Kondo(1986):

$$
\begin{aligned}
\phi_{mn}(\sigma) \quad = \quad & \int_{\boldsymbol{k}} H_m(\boldsymbol{k}, \sigma)\, H_n(\boldsymbol{k}, \sigma) S(\boldsymbol{k}, \sigma) \times \\
& [\ \exp\{-\boldsymbol{k} \cdot (\boldsymbol{x}_n - \boldsymbol{x}_m)\} + r^2 \exp\{-\boldsymbol{k} \cdot (\boldsymbol{x}_{nr} - \boldsymbol{x}_{mr})\} + \\
& r \exp\{-\boldsymbol{k} \cdot (\boldsymbol{x}_{nr} - \boldsymbol{x}_m)\} + r \exp\{-\boldsymbol{k} \cdot (\boldsymbol{x}_n - \boldsymbol{x}_{mr})\}\,]\, d\boldsymbol{k} \quad (11)
\end{aligned}
$$

where $r$ is the reflection coefficient, $\boldsymbol{x}_{nr}$ and $\boldsymbol{x}_{mr}$ are symmetrical space vectors of $\boldsymbol{x}_n$ and $\boldsymbol{x}_m$ against the reflecting boundary, and $\boldsymbol{k}$ is a wave number vector of the incident waves defined in a half domain.

The coherence function in the combined wave field can be calculated by the above equation. Fig.2 is an example of the coherence distribution in space domain between the origin and any other position in the half domain under the condition of $r = 1.0$ and $\theta_0 = \pi$.    In Fig.2, the coherence value along the wave direction changes very rapidly at the nodal position and gives the maximum value at the anti-nodal position. This figure shows that the coherence distribution in space domain would be useful to evaluate the wave spreadings in the combined wave field.

# 3    Experimental set-up

The dimension of the wave basin is 45m wide, 35m long and 1.1m deep (Fig.3). The absorbing directional wavemaker consistes of 48 wave paddles, each of which is controlled independently and is 40cm wide and 120cm high (Hirakuchi et al., 1990a). To detect the reflected waves, a capacitance wave gauge is mounted on the front side of each paddle. It is possible to switch the absorption loop in or out of the control circuit, so this wavemaker also work as a conventional wavemaker. The absorbing principle and its performance for the uni-directional irregular waves in a wave channel have been described and examined by Hirakuchi et al.(1990b).

To examine the performance of wave generation and reflected wave absorption, all four combinations of the following alternatives are considered in the experiments:   1) either with or without the absorption loop, and 2) either with or without the remarkable reflected waves in the basin (with the vertical wall in Fig.4, with absorbing beach in Fig.3).

Regular and irregular wave experiments are carried out at the water
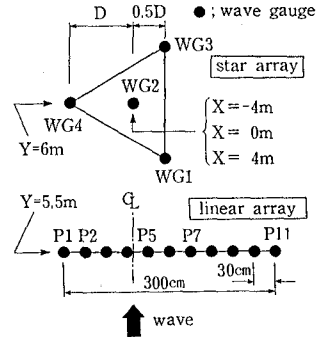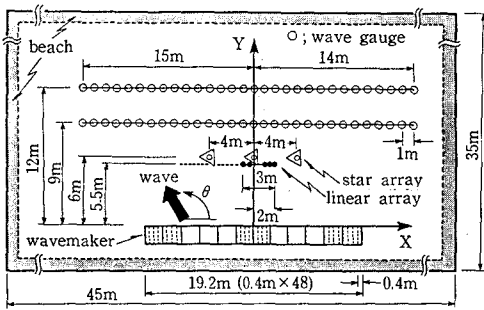
(a) wave basin and wavemaker                    (b) wave gauges

**Fig.3**  Experimental set-up for the progressive wave generation. Absorbing beach is settled aroud the basin to reduce the reflected waves from the side wall of the basin.
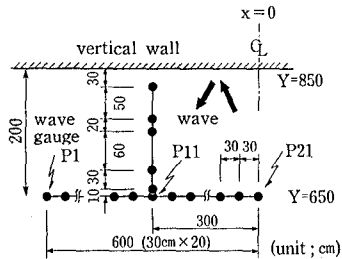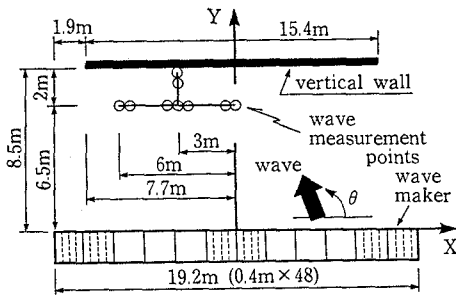


(a) reflective vertical wall                    (b) wave gauges

**Fig.4**  Experimental set-up for the combined wave field. The reflection coefficient at the vertical wall is 1.0.

depth of 50cm. The wave height and period used for regular wave experiments are H=4~5cm and T=1.0~1.5s. For the directional wave experiments, the Mitsuyasu-type angular spreading function and the Bretschneider-type power spectrum are used as a target spectrum. The significant wave height and period for $s_{max}$=10 and 75 are $H_{1/3}$=5.0, 4.0cm and $T_{1/3}$=1.0, 1.25s, respectively. The double-summation model are used for the wave synthesis.

The star arrays in Fig.3 and the linear array in Fig.3 and 4 are used for the directional specrtum analysis. The linear array in Fig.3 and 4 are also used to evaluate the coherence distribution in space and frequency domain.

# 4    Results for progressive wave fields

## 4.1    Regular waves

Firstly, experiments on oblique regular waves were curried out (see Fig.3), and the generated waves were compared with the numerical and analytical results. Fig.5 is an example of the wave height distribution at y=9m in Fig.3. The black circle is the experimental result, and the break line and the solid line are analytical result proposed by Takayama(1982) and the numerical result calculated by the mild slope equation, respectively. The mild slope equation used in this study is:

$$\left.\begin{array}{l} \dfrac{\partial \boldsymbol{Q}}{\partial t} + C^2 \nabla \zeta = 0 \\[4mm] \dfrac{\partial \zeta}{\partial t} + \dfrac{1}{n}\nabla \cdot (n\boldsymbol{Q}) + \dfrac{f_d}{n}\zeta = 0 \end{array}\right\} \tag{12}$$

where $C$ is the wave velocity, $\zeta$ is the surface elevation, $f_d$ is a coefficient for energy dissipation, and $n$ and $\boldsymbol{Q}$ are defined as:

$$n = C_g/C \;\; = \;\; \frac{1}{2}\left(1 + \frac{2kh}{\sinh 2kh}\right) \tag{13}$$

$$\boldsymbol{Q} \;\; = \;\; \int_{-h}^{0} \boldsymbol{U}\, dz \tag{14}$$

in which $\boldsymbol{U}$ is the water particle velocity.

Eq.(12) is equivalent to the mild slop equation with the dissipation term $f_d$ (Dalrymple, Kirby et al., 1984):

$$\nabla \cdot (nC^2\nabla\zeta) + n\sigma^2\zeta + i\sigma f_d\zeta = 0 \tag{15}$$

Fig.5 shows good agreement between the measured wave heights and the numerical results calculated by Eq.(12). It is notified that the analytical result proposed by Takayama is not satisfied with the experimental boundary condition illustrated in Fig.3.
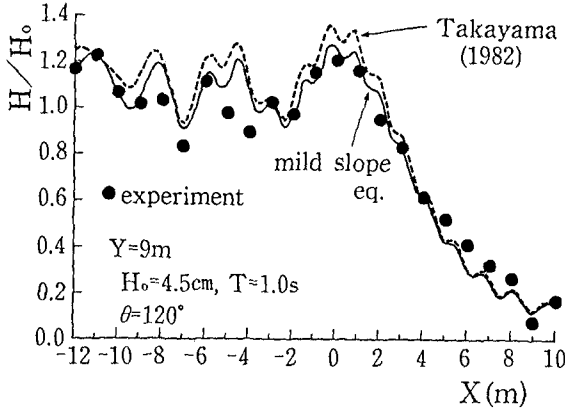
**Fig.5** Wave height distribution of oblique waves in the progressive wave field. ● represents the measured value at Y=9m, the dotted line is the analytical value by Takayama and the solid line is the numerical value calculated by the mild slope equation.



(a) $s_{max} = 10$           (b) $s_{max} = 75$
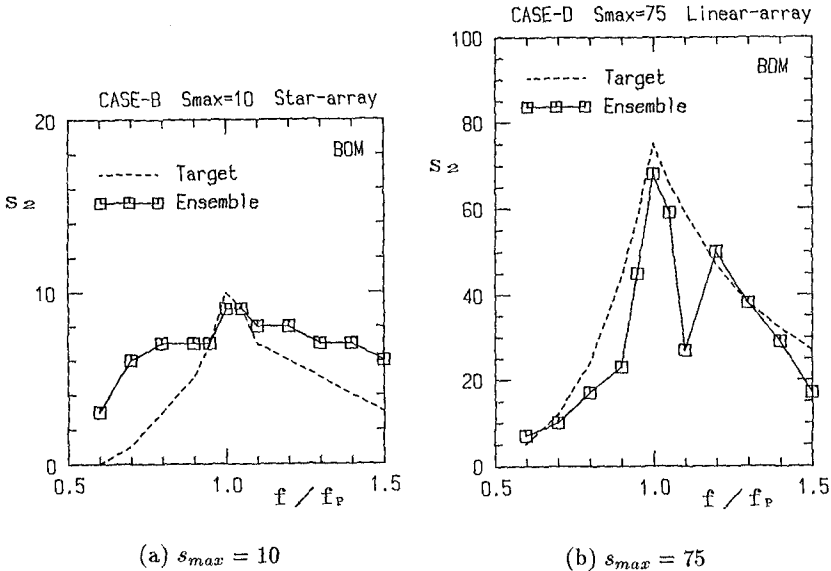
**Fig.6** Comparison between estimated angular spreading parameter and target one. □ is estimated by Eq.(16) using the directional spectrum analysed by BDM. For the BDM analysis, the averaged cross spectrum for 6 experiments are used.

## 4.2    Directional waves

Directional wave experiments with $s_{max}$ =10 and 75 are carried out. In order to reduce the statistical variation, six experiments are carried out, each of which has the same wave parameters but has different ramdom phases. Using the averaged cross spectrum for the six experiments, the directional spectrum is analysed by the Bayesian Model (BDM) proposed by Hashimoto and Kobune(1987b). The spreading parameter of the analysed directional spectrum is calculated by the following form:

$$s = \left(\frac{1}{\gamma^2} - \frac{1}{2}\right) + \left(\frac{1}{\gamma^4} - \frac{3}{4}\right)^{1/2} \tag{16}$$

where $\gamma$ is a long-crested parameter at a frequency $f$

$$\gamma(f) = \left[\frac{(M_{20} + M_{02}) - \sqrt{(M_{20} - M_{02})^2 + 4M_{11}^2}}{(M_{20} + M_{02}) + \sqrt{(M_{20} - M_{02})^2 + 4M_{11}^2}}\right]^{1/2} \tag{17}$$

$$M_{pq}(f) = P(f)\int_0^{2\pi}(k\cos\theta)^p(k\sin\theta)^q G(f,\theta)d\theta \quad ;p,q = 0,1,2 \tag{18}$$

Fig.6 is the estimated results of $s$, where the dotted line is the target one defined in Eq.(3) and □ is the measured one calculated by Eq.(16). The estimated values of $s$ show good agreement with the target ones, although the some results for $s_{max}$=75 show the small values.

The coherence distribution between P1 and P2∼P11 (in Fig.3) are measured. Fig.7(a) gives the result along the crest line ($\alpha = 0°$) at the peak frequency of the long-crested waves: the target value of $s$ at the peak frequency is $s$=75. The solid line is the coherence function of the target waves, □ is the coherence value of the averaged cross spectrum, and the other six marks represent the coherence values of the six expriments. The agreement between the averaged value and the target value is very good, although the measured value for each experiment varies from $s = 30 \sim 150$.

The coherence distribution in frequency domain are also calculated. Fig.7(b) gives the coherence between P1 and P3 along the crest line with the distance of 60cm. The solid line is the coherence value of the averaged cross spectrum, and the dotted line with ● is the coherence value of the target wave with the Mitsuyasu-type spreading function. The averaged coherence value shows good agreement with the expected one.

case-D0  [ $\alpha = 0^\circ$,  base:P1,  f/fp=1.0 ]
                    [ DS-model,  Smax=75 ]

case-D0  [ $\alpha = 0^\circ$,  R=60cm (P1-P3) ]
                    [ DS-model,  Smax=75 ]

(a) coherence in space domain     (b) coherence in frequency domain
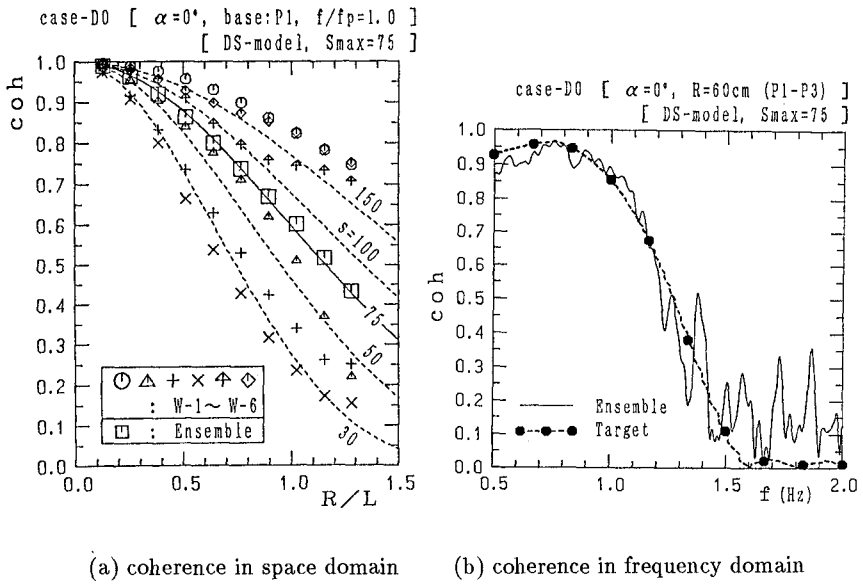
**Fig.7**  Coherence value measured in progressive wave field ($s_{max} = 75$).

[ H0=5.65cm,  T=1.5s,  $\theta = 105^\circ$ ]

【 with absorption loop 】

P 2 1     (x, y) = (0m, 6.5m)

P 1     (x, y) = (-6m, 6.5m)

【 without absorption loop 】

P 2 1     (x, y) = (0m, 6.5m)

P 1     (x, y) = (-6m, 6.5m)
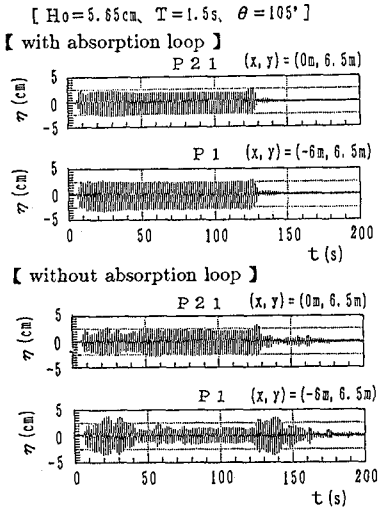
**Fig.8**  Time histories of generated oblique waves ($\theta = 105^\circ$) with and without the absorption loop in the combined wave field.
P1 and P21 are shown in Fig.4

# 5   Results for combined wave fields

## 5.1   Regular waves

To reproduce the incident and reflected combined wave field, a vertical wall with the reflection coefficient of 1.0 are settled as shown in Fig.4. 21 wave gauges (P1~P21) are arranged parallel to the wall and 6 wave gauges are arranged perpendicular to the wall.

Experiments on oblique regular waves were carried out with and without the absorption loop. The time history measured at P1 and P21 are shown in Fig.8. The upper and lower two graphes represent the result with and without the absorption loop, respectively. The waves generated without the absorption loop are unstable, and the multi-reflected waves between the wall and the wavemaker are apparently remained over the range of $t > 125$s.

Fig.9 is the result of the wave height distribution along the parallel and perpendicular line to the wall, generated with the absorption loop. $\square$, $\bigcirc$ and $\triangle$ are the mean wave heights during several wave periods (T). $\square$ is the early result of the combined wave field, which may not be affected by the multi-reflected waves. The break line and the solid line are the numerical results of the expected combined wave field calculated by Eq.(12). Fig.9 shows that the wave heights along the both lines are rather stable in time and agree to the expected results.

## 5.2   Directional waves

Directional wave experiments with $s_{max}=10$, 75 and $\infty$ are carried out with and without the absorption loop, and the combined wave fields are reproduced. The significant wave height along the perpendicular line to the wall are shown in Fig.10. This figure shows that the results with the absorption loop are not affected by the reflected waves. Since the reflection coefficient at the vertical wall is 1.0, the ratio of the significant wave height $(H/H_0)$ may be equal to 2.0 at the wall and to $\sqrt{2}$ at large distances from the wall, and the minimum value may be occured at Y≈8m (L/4 away from the wall). The agreement with the measured results with the absorption loop and the theoretical values mentioned above is also excellent.

Fig.11 gives the comparison of the directional spectrum with and without the remarkable reflected waves in the basin: Fig.11(a) and (b) are the power spectrum and the directional spreading function, respectively. These results show that the directional spectrum of the incident waves in the combined wave field is not affected by the re-reflected waves at the paddles.

Fig.12 is an example of the coherence distribution along the pararelle line (P1~P21) in Fig.4. $\bigcirc$ represents the coherence value between P11 and

[ Ho = 5.65cm,  T = 1.5s,  $\theta$ = 105' ]  Y = 6.5m

Y=6.45m
Y=6.5m

$\square$ : $t = 1 \sim 4T$
$\bigcirc$ : $t = 10 \sim 14T$
$\triangle$ : $t = 25 \sim 29T$

Y=6.55m

(a) Y= 6.5m
(paralell to the wall)

X = −3 m

vertical wall (Y=8.5m)
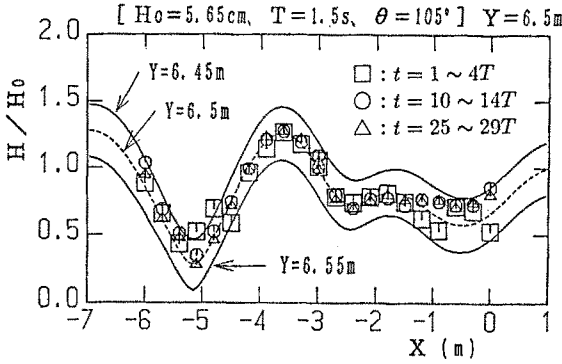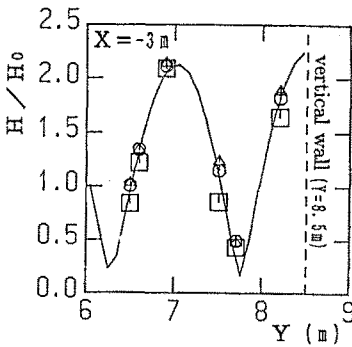
(b) X= −3m
(parpendicular to the wall)

**Fig.9** Comparison between wave height in the combined wave field generated with the absorption loop and numerical results of the mild slope equation (solid and dotted lines).
$\square$, $\bigcirc$ and $\triangle$ are measured values.

| abs. | S m a x |
|------|----|----|----|
| loop | 10 | 75 | ∞ |
| off  | ● | ■ | ▲ |
| on   | ○ | □ | △ |
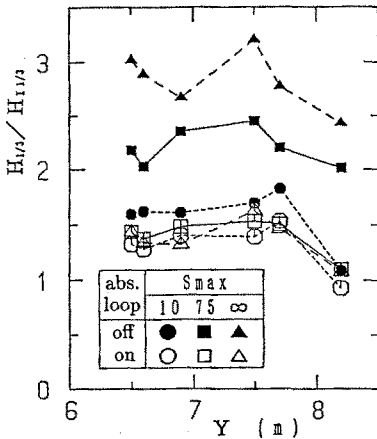
**Fig.10** Comparison of the significant wave height in the combined wave field ($s_{max} = 10, 75, \infty$).
The white and black marks represent experimental results with and without the absorption loop, respectively.
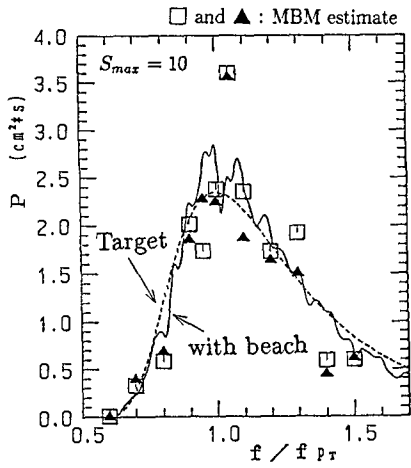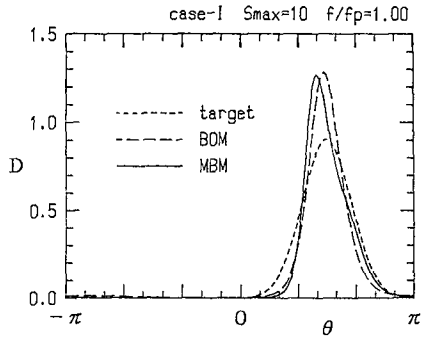
(a) power spectrum                    (b) angular spreading function

**Fig.11**  Comparison of directional spectrum with and without the remarkable reflected waves in the basin.  □ and ▲ represent the power spectrum of the incident waves in the combined wave field. These two results are estimated by MBM using the data measured at the different position.
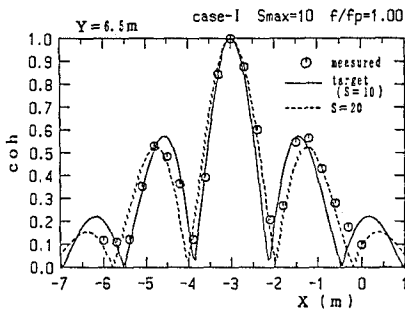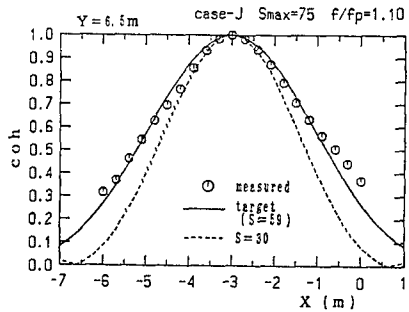


(a) $s_{max} = 10$, $f/f_p = 1.0$             (b) $s_{max} = 75$, $f/f_p = 1.1$

**Fig.12**  Comparison of coherence distribution in space domain in the combined wave field. ○ represents the obseved coherence value between P11 (; x=−3m) and P1∼P21(; x=−6∼0m), and solid line represents the theoretical value of the target combined wave field.

P1~P21, so the coherence at P11 ($x = -3$m) is equal to 1.0. Fig.12(a) is the result for $s_{max}=10$ at $f/f_p=1.0$, and Fig.12(b) is the result for $s_{max}=75$ at $f/f_p=1.1$. The measured coherence value agrees very well to the expected value.

# 6   Conclusion

The absorbing directional wavemaker has been developed, and its performance is examined experimentally. Several experiments were carried out either with or without the absorption loop in the progressive wave field and in the combined wave field. From the comparison of the wave height, the directional spectrum and the coherenc function of the cross spectrum, it is shows that the absorbing directional wavemaker has excellent performance to absorb the reflected waves. The wavemaker can reproduce the short- and long-crested waves with the specific directional spectrum, and can maintain the better controlled incident wave field.

## REFERENCES

**Dalrymple, R.A., J.T. Kirby and P.A. Hwang (1984)** : Wave diffraction due to area of energy dissipation, *Proc. ASCE*, Vol.110, No.WW1, pp.67–79.

**Hashimoto, N. et al.(1987a)** : Estimational spectra from a Bayesian approach in incident and reflected wave field, *Report of Port and Harbour Research Inst.*, Vol.26, No.4, pp.3–33 (in Japanese).

**Hashimoto, N. and K. Kobune (1987b)** : Estimation of directional spectrum using the Bayesian approach, and its apprication to field data analysis, *Report of Port and Harbour Research Inst.*, Vol.26, No.5, pp.57–100.

**Hirakuchi, H. et al. (1990a)** : Laboratory measurement and generation of directional water waves, *Proc. 37th Japanese Conf. Coastal Eng.*, pp.150–154 (in Japanese).

**Hirakuchi, H. et al. (1990b)** : Application of a piston-type absorbing wavemaker to irregular wave experiments, *Coastal Eng. Japan*, Vol.33, No.1, pp.11–24.

**Isobe, M. and K. Kondo (1986)** : Method for estimating directional wave spectrum in incident and reflected wave field, *Proc. 19th ICCE*, pp.467–483.

**Takayama, T. (1982)** : Theoretical properties of oblique waves generated by serpent-type wave-maker, *Report of Port and Harbour Research Inst.*, Vol.21, No.2, pp.3–48.